

Using Reconstructed IVUS Images for Coronary Plaque Classification

Karla L. Caballero, Joel Barajas, Oriol Pujol, Oriol Rodriguez and Petia Radeva

Abstract—Coronary plaque rupture is one of the principal causes of sudden death in western societies. Reliable diagnostic of the different plaque types are of great interest for the medical community the predicting their evolution and applying an effective treatment. To achieve this, a tissue classification must be performed. Intravascular Ultrasound (IVUS) represents a technique to explore the vessel walls and to observe its histological properties. In this paper, a method to reconstruct IVUS images from the raw Radio Frequency (RF) data coming from ultrasound catheter is proposed. This framework offers a normalization scheme to compare accurately different patient studies. The automatic tissue classification is based on texture analysis and Adapting Boosting (Adaboost) learning technique combined with Error Correcting Output Codes (ECOC). In this study, 9 *in-vivo* cases are reconstructed with 7 different parameter set. This method improves the classification rate based on images, yielding a 91% of well-detected tissue using the best parameter set. It also reduces the inter-patient variability compared with the analysis of DICOM images, which are obtained from the commercial equipment.

I. INTRODUCTION

Cardiovascular diseases are some of the principal causes of sudden death in the western societies. It has been observed that several pathologies are caused by the plaque rupture from the coronary vessels. Thus, an accurate detection of the plaque susceptible to rupture is of great relevance for the medical community [Burke et al., 1997].

Intravascular Ultrasound (IVUS) images offer us the opportunity to classify the coronary plaque, since they display the morphology and the histological properties from a cross-section of the vessel, which offer us a unique view of the arterial plaque. In these images, three different plaques are distinguishable: calcified (characterized by a very high echo-reflectivity and signal absorption); fibrotic (medium echo-reflectivity and good transmission coefficient) and lipidic or soft plaque (very low reflectance)[Zhang et al., 1998]. The automatic analysis of these tissues in IVUS images represents a feasible way to predict a quantify the vulnerable plaques[Zhang et al., 1998], [Pujol et al., 2003], avoiding the subjectivity due to the high intra-observer variability

This work was supported in part by a research grant from projects TIN2006-15308-C02, FIS-PI061290, by the Generalitat of Catalunya under the FI grant and by the Spanish Ministry of Education and Sciences (MEC) under the FPU grant Ref: AP2005-0926

K. L. Caballero and Joel Barajas are with the Computer Vision Center, Autonomous University of Barcelona, Edificio O Campus UAB, 08193 Bellaterra, Spain klcaballero@cvc.uab.es, joelbz@cvc.uab.es

Oriol Pujol and Petia Radeva are with the Department Mathematical Analysis, University of Barcelona, Barcelona, Spain and the Computer Vision Center. oriol@maia.ub.es, petia@cvc.uab.es

Oriol Rodriguez is with the Hemodynamics Department, Hospital Universitari German Trias i Pujol, Badalona, Spain

of this study. Additionally, it allows to reduce the processing time spent in characterizing large sequences of images.

One of the main problems of working with the IVUS images come from the acquisition of normalized DICOM images, since each physician can acquire them with different offset parameters. Additionally, once these images are recorded is not possible to change their contrast, since they are equalized radially with a non linear model, and the image parameters are not often available. This lack of normalization hinders the automatic classification since the tissues from different patients may not be comparable due to the divergence in image contrast and radial depth.

This paper proposes a reconstruction of IVUS images from the Radio Frequency (RF) signals coming from the catheter of the IVUS equipment. This offers us the opportunity of normalizing different pullbacks with a fixed parameter set. Furthermore, we can select the contrast which provides higher accuracy and lower variability among patients.

This paper is organized in the following manner: in section 2 a comparison among DICOM and reconstructed images is detailed. Then, in section 3 the reconstruction process is explained. The feature extraction by using texture descriptors is shown in section 4. The classification scheme is presented in section 5. Finally, results and conclusion are given.

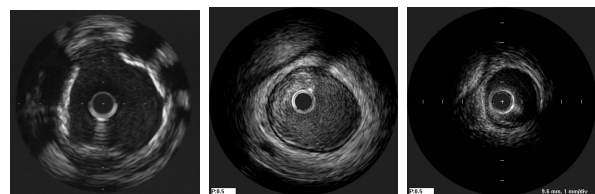


Fig. 1. DICOM images with different contrast and radial depth

II. DICOM VS. RECONSTRUCTED IMAGE

When an IVUS study is performed, DICOM images are generated by the ultrasound equipment. These images are recorded with a specific setting of image acquisition parameters. To improve the visualization of certain tissues in the IVUS image, physicians change the imaging parameter set (*i.e.* contrast and depth of the image). This procedure may hinder the image classification, since a given type of plaque can be visualized differently, making them non comparable. Figure 1 shows DICOM images from three patients saved with different parameter sets. Furthermore, the images can not be adjusted to a fixed parameter set, since the reconstruction information, the RF signals and the visualization parameters used are not saved.

Reconstructed IVUS images represent a feasible form to keep all the image information. This is achieved by saving the RF signals coming from the IVUS equipment. The parameters of the image can be changed easily without a loss of information with different contrast and depth to simplify a multi-observer study or to perform automatic analysis with a fixed parameter set.

III. IMAGE RECONSTRUCTION PROCESS

An IVUS equipment consists of a main computer and a catheter which is introduced into the vessel to perform an exploration. This catheter carries an ultrasound emitter that shoots a given number of beams, and a transducer that collects their reflections as RF signals. Based on the kind of tissue, these signals vary their frequency and amplitude.

The RF signals are acquired using a 12-bit Acqiris acquisition card with a sampling rate of $200MHz$. The frequency of the catheter transducer is $40MHz$, and a sound speed in tissue of $1565m/s$ is assumed. Each IVUS image consists of a total of 256 A-lines (ultrasound beams), and a length of $4.9mm$. The RF data were acquired from patient pullback sequences *in vivo*.

Then, the signals are filtered with a band pass filter located at the transducer frequency. This is done to eliminate the signals which do not come from the transducer response. In order to correct the attenuation of the reflected ultrasound wave in tissue, a time gain compensation is applied assuming an attenuation factor of $\alpha = 1DbMHz/s$. After the signals are compensated their envelope is calculated employing the Hilbert transform. This envelope is compressed in logarithmical form to distribute the values in the histogram and enhance the visualization and normalized in a range of 0 to 1. Then each of the beams is arranged into a polar image. The image is constructed into its cartesian form and the missing pixels between each angle are filled interpolating the gray scale values of the neighbors.

Then, a non linear Digital Development Process (DDP)[Gonzales and Woods, 1992] is applied in order to regulate the contrast radially. The parameters are fixed in order to normalize all the images with the same contrast. This step consists in dividing the cartesian image radially in several sections which are normalized and filtered separately according to the interpolation level. Then, a weighted contrast is applied to uniform all the image such that its distribution in the image along the radius is fixed and only one logarithmic parameter gain K is changed. Figure 2(a) shows a DICOM image compared with reconstructed ones with different K parameters and the same depth shown in figure 2(b),(c). Reconstructed images are used to perform the classification with a texture based approach, the visualization and the manual segmentation of the images.

IV. TEXTURE FEATURES EXTRACTION

To extract the features in the image 4 different texture descriptors are used: co-occurrence matrices, local binary patterns, Gabor filters and the shading of the polar image.

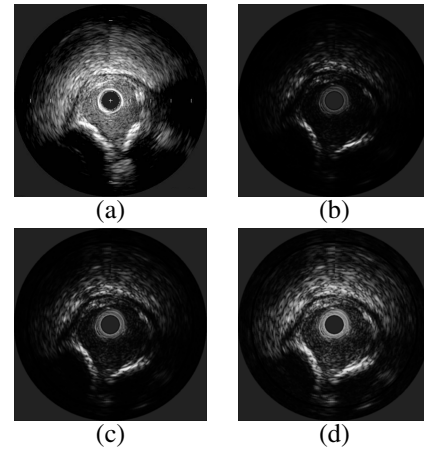


Fig. 2. Reconstructed IVUS images from RF signals with different DDP gain parameters K . (a)DICOM image from the IVUS equipment.(b)DDP gain parameter fixed to 1.04. (c)DDP gain parameter fixed to 2.20. (d)DDP gain parameter fixed to 3.40.

The co-occurrence matrix can be defined as an estimation of the joint probability density function of gray level pairs in an image [P. Ohanian, 1992]. The element values in the matrix are bounded from 0 to 1 and their sum is:

$$P(i, j, D, \theta) = P(I(l, m) = i \otimes I(l + D\cos(\theta), m + D\sin(\theta)) = j),$$

where $I(l, m)$ is the gray value at the pixel (l, m) , D is the distance among pixels and θ is the angle of each of its neighbors. The angle orientation θ has been fixed to be $[0^\circ, 45^\circ, 90^\circ, 135^\circ]$. According to [Husoy, 1999], [P. Ohanian, 1992], it is the minimum set of orientations needed to describe a second-order statistic measures of texture. After computing this matrix six characterizing measures are extracted as defined in [P. Ohanian, 1992]. Thus, a 48 feature space is built for each pixel, since we are estimating 6 different measures at 4 orientations and two distances $D = [5, 8]$.

The Local Binary Patterns are used to detect uniform texture patterns into circular neighborhoods with any quantization of angular space and spatial resolution [Ojala and Maenpaa, 2002]. They are based on a circular symmetric neighborhood of P members of a circle with radius R . Gray level invariance is achieved when the central pixel g_c is subtracted to each neighbor g_p , assigning to the result 1 if the difference is positive and 0 if it is negative. Each neighbor is weighted with a 2^p value. Then, the neighbors are added, and the result is assigned to the central pixel. With these operators we generate a 3 dimensional space, by applying a radius of $R = [1, 2, 3]$ and a neighborhood of $P = [8, 16, 24]$.

The Gabor Filters are a special case of wavelets [Daugman, 1985]. They can be defined as a Gaussian g modulated by a complex sinusoid s . In 2D, a Gabor filter has the following form in the spatial domain:

$$h(x, y) = \frac{1}{2\pi\sigma_x'\sigma_y'} \exp\{-\frac{1}{2}[(\frac{x'}{\sigma_x'})^2 + (\frac{y'}{\sigma_y'})^2]\} \cdot s(x, y),$$

where $s(x, y)$ and the Gaussian rotation are defined as:

$$s(x, y) = \exp[-i2\pi(Ux + Vy)]$$

$$x' = x \cos \theta + y \sin \theta, \quad y' = -x \sin \theta + y \cos \theta.$$

x' and y' represent the spatial coordinates rotated by an angle θ . $\sigma_{x'}$ and $\sigma_{y'}$ are the standard deviations for the Gaussian envelope. The aspect ratio λ and its orientation are defined as:

$$\lambda = \frac{\sigma_{x'}}{\sigma_{y'}}, \quad \phi = \arctan V/U$$

where U and V represent the 2D frequencies of the complex sinusoid.

λ has been fixed to create isotropic gaussian envelopes, resulting that $\sigma_{x'} = \sigma_{y'}$, and θ is discarded. The 2D frequency, (U, V) has been changed to its polar representation F, ϕ . We have created a filter bank with the following parameters:

$$\sigma_x = \sigma_y = [12.7205, 6.3602, 3.1801, 1.5901],$$

$$\phi = [0^\circ, 45^\circ, 90^\circ, 135^\circ],$$

$$F = [0.0442, 0.0884, 0.1768, 0.3536],$$

yielding a 16 dimensional space for each pixel.

According to [Zhang et al., 1998], one of the main differences in the calcified tissue is the shadow which is appreciated behind it in the radial direction. In order to detect this shadow, we performed the accumulative mean of the polar image. This measure is obtained by calculating the mean, from one pixel to the end of the column. Before calculating this, we chose a threshold to give the same weight to the tissue and a lower one to the shadow.

We compiled all the features extracted above into a vector of 68 dimensions for each pixel. These will be used to train the classifier. The main idea is to extract the best of each technique in order to improve the classification performance.

V. CLASSIFICATION

Once we designed a characterization framework, a classification scheme is developed. We consider 3 classes of tissue: fibrotic, lipidic and calcified. We use the Adaptive Boosting (Adaboost) with decision stumps as supervised learning technique.

Adaboost allows us to add "weak" classifiers until some desired training error is obtained [Schapire, 2001]. In each step of the algorithm a feature is chosen and assigned a certain weight, which means how accurate this feature can classify the training data. As a result linear combination of weaker classifiers is obtained.

Since this method trains binary classifiers and we have a multiclass problem, we need to establish a criterion for the different classifiers output. To achieve this, we employ Error Correction Output Codes (ECOC) [Allwein et al., 2000]. This consists in assigning a code map table which relates classifiers outputs and classes. Then, the final classification is obtained finding the minimum distance between the sample code and classes code.

The ECOC classification map is shown in table I. Here, the number 0 indicates that these classes are not used by the selected classifier. The 1 indicates that the classifier should output a positive value when this class is found, and negative one (-1) when it is not.

Once the classification results are obtained, the Euclidean distance is found between each sample of the test and all the

TABLE I
ECOC CODE MAP USED IN THE CLASSIFICATION

Classes	Classifiers					
	h1	h2	h3	h4	h5	h6
Calcium	1	1	0	1	-1	-1
Fibrotic Plaque	-1	0	1	-1	1	-1
Soft Plaque	0	-1	-1	-1	-1	1

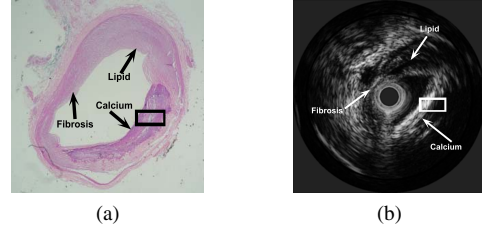


Fig. 3. Correlation between histologic and IVUS images

class codes. Thus, the class with the minimum distance with respect to the sample is assigned to it.

VI. RESULTS

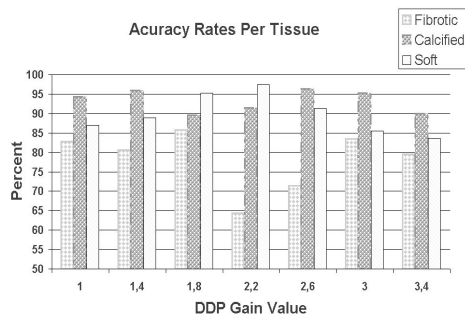
We reconstructed IVUS images from a set of 9 patients all of them containing the three classes of plaque. Each patient may have 1 or 2 vessel studies or pullbacks. Then, for each one, 10 to 15 different vessel sections or images are selected to be analyzed. Additionally we have tested our framework with 6 *ex vivo* cases validated with histological studies. Figure 3 shows an IVUS image and its respective histological image.

We developed an approach to construct IVUS images from the RF signals. This has the advantage of allowing the physicians to move the contrast parameter of the reconstructed image to simplify the manual segmentation task. Although the main purpose of this step is to segment the training data and label it, the gain offset K used for the segmentation is stored for future analysis.

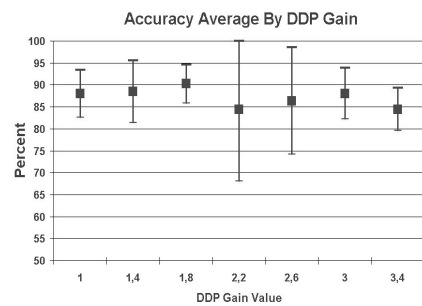
Two physicians segmented independently from the vessel images 50 sections of interests per patient. The regions where both agreed to be the same tissue were taken as regions of interest (ROI) which were collected into a database categorized by patient. These were mapped in the reconstructed images to build the data set.

The experiment has been validated using Leave One Patient Out method which consists in picking one different patient for testing and the rest for training purposes. It is done to avoid any possible bias resulting from testing the classification with the same information of the training set. In addition, this gives us an idea of how the classification could behave with a new patient.

The performance of the classification approach in the *in vivo* cases was tested by selecting 7 different K values of the DDP gain (contrast) to reconstruct the images. Therefore, 7 different data sets have been created, and their features extracted have been processed separately. For each DDP gain parameter value, a classification error rate has been calculated for every type of tissue.



(a)



(b)

Fig. 4. a) Classification rate among different DDP gain parameters for each type of tissue with leave-one-patient-out method. b) Classification accuracy among the different tissue types

The accuracy for all the different DDP gain parameters is shown in figure 4(a). Additionally, the global accuracy for each contrast value is calculated among all the patients. This is shown in figure 4(b). In these graphs can be observed that the best classification accuracy is achieved with the gain equal to 1.8, since this value offers the highest average in the classification hit rate and the smaller variability among different patients. The gain equal to 2.2 gives a similar accuracy rate, but the variability among the different patients is highly significant, which can hinder the classification result with a new patient.

The classification accuracy rate for the *ex vivo* studies with the best gain is: 80,06% for fibrotic, 94,72% for soft and 99,38% for calcified tissue. This result is highly correlated with the obtained with the *in vivo* samples which shows the repetitiveness and robustness of the method.

The accuracy rates presented here represent an improvement in the tissue characterization problem respect to the DICOM based approaches. Usually, the classification rates reported in these approaches are around 76% of the total performance without any kind of postprocessing [Pujol, 2004], [Zhang et al., 1998]. The difference is mainly caused by the use of normalized data to test our classification framework. Figure 5 shows the result of the automatic classification using the best gain obtained. Here, it can be seen that the classification result compared with the physician's segmentation is highly correlated.

VII. DISCUSSION AND CONCLUSION

A new method for tissue classification using IVUS images from *in vivo* patients has been presented. We propose a more

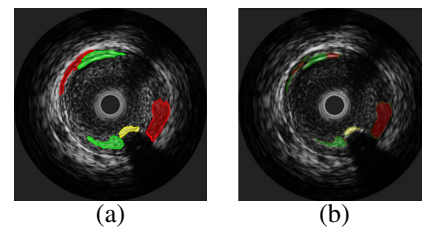


Fig. 5. Image classification result a)Image segmented by the physician, b)Classification Result using the best gain

accurate technique based on a set of normalized data, which is not possible in conventional approaches based on DICOM images. To do so, an image reconstruction method has been depicted and adapted to the characterization process.

As a result the hit rate of the classification is higher in reconstructed images than in DICOM images. Additionally, we apply successfully a multi-class problem as a combination of binary classifiers based on discrete Adaboost using ECOC.

The classification presented here has been done for each pixel and without any kind of postprocessing. This is done to preserve the highest possible resolution. However, to generalize the response for a tissue some grouping techniques could be applied. Additionally, performing this grouping, the mixed plaque can be defined. This has not been defined yet at the class level, since the mixed plaque is a combination of the 3 principal plaques presented. The use of Radio Frequency signal can complement this framework, since it represents the raw data and the real response of the tissue

REFERENCES

- [Allwein et al., 2000] Allwein, E. L., Schapire, R. E., and Singer, Y. (2000). Reducing multiclass to binary: A unifying approach for margin classifiers. *Journal of Machine Learning Research*, 1:113–141.
- [Burke et al., 1997] Burke, A. P., Farb, A., hui Liang, G. T. M. Y., Smialek, J., and Virmani, R. (1997). Coronary risk factors and plaque morphology in men with coronary disease who died suddenly. *The New England Journal of Medicine*, 336(18):1276–1281.
- [Daugman, 1985] Daugman, J. (1985). Uncertainty relation for resolution in space, spatial frequency, and orientation optimized by two-dimensional visual cortical filters. *Journal of the Optical Society of America*, 2(A):1160–1169.
- [Gonzales and Woods, 1992] Gonzales, R. and Woods, R. (1992). *Image Processing*. Adison - Wesley.
- [Husoy, 1999] Husoy, T. R. J. H. (1999). Filtering for texture classification: A comparative study. *IEEE Transactions on Pattern Analysis and Machine Intelligence*, 4:291–310.
- [Ojala and Maenpaa, 2002] Ojala, T. and Maenpaa, M. P. T. (2002). Multiresolution gray-scale and rotation invariant texture classification with local binary patterns. *IEEE Transactions on Pattern Analysis and Machine Intelligence*, 24:971–987.
- [P. Ohanian, 1992] P. Ohanian, R. D. (1992). Performance evaluation for four classes of textural features. *Pattern Recognition*, 25:819–833.
- [Pujol, 2004] Pujol, O. (2004). *A semi-supervised Statistical Framework and Generative Snakes for IVUS Analysis*. Graficas Rey.
- [Pujol et al., 2003] Pujol, O., Rosales, M., and Radeva, P. (2003). Intravascular ultrasound images vessel characterization using adaboost. In *Functional Imaging and Modelling of the Heart: Lecture Notes in Computer Science*, pages 242–251.
- [Schapire, 2001] Schapire, R. (2001). The boosting approach to machine learning: An overview.
- [Zhang et al., 1998] Zhang, X., McKay, C. R., and Sonka, M. (1998). Tissue characterization in intravascular ultrasound images. *IEEE transactions on Medicine*, 17(A):889–898.